

Biomechanical and Physical Properties Selection of Ti-Ha-CaCO₃ Biocomposite Prostheses for Replacement of Bone Atrophy

H. K. Ibrahim^{1,3*}, M. S. Abolarin¹, A. S. Abdulrahman², O. Adedipe¹, U. G. Okoro¹

¹Department of Mechanical Engineering, Federal University of Technology Minna, Nigeria.

²Department of Material and Metallurgical Engineering, Federal University of Technology Minna, Nigeria.

³Department of Mechanical Engineering, University of Ilorin, Nigeria.



ABSTRACT: Traditional prosthetic materials often lack the desired properties to mimic the mechanical behaviour of natural bone, leading to complications and reduced implant longevity. This study aims to conduct a biomechanical and physical properties selection analysis for biocomposite prostheses' suitable for replacing bone atrophy. This involves evaluating the mechanical properties of developed biocomposites with different structures (dense, porous and gradient) to ensure compatibility with the mechanical properties of bone. The radar chart was adopted to compare and evaluate the mechanical strength of various biocomposite implants and identify the most suitable prosthesis for load-bearing bone replacement. The study utilises powder metallurgy, scanning electron microscopy (SEM), and ImageJ software to produce and characterise the pore size distribution of the biocomposites, respectively. The findings of this study revealed the gradient and porous biocomposites exhibited desired mechanical properties with porosity of 20.67 and 27.72 % pore size up to 134 and 256 μm , compressive strength of 174 and 149.29 MPa and compressive modulus of 30.42 and 28.3 GPa respectively. The SEM analysis, coupled with pore size distribution and porosity percentage measurements, offers valuable information for designing and fabricating biomaterials with enhanced properties. The gradient biocomposite was identified to be the best sample for load-bearing bone replacements by the selection analysis because of its high compressive strength and low modulus, which is within the established cortical bone mechanical properties.

KEYWORDS: Biocomposite, Biomechanical, Structure, Properties, Prosthesis, ImageJ

[Received Nov. 19, 2023; Revised Jan. 7, 2024; Accepted Jan. 14, 2024]

Print ISSN: 0189-9546 | Online ISSN: 2437-2110

I. INTRODUCTION

A decrease in bone mass and density characterise bone atrophy, a common condition affecting individuals due to various factors such as ageing, accident, trauma, or disease. In severe cases, load-bearing bones may become significantly compromised, necessitating prostheses for bone replacement (Bahraminasab and Farahmand, 2017). According to the Food and Drug Administration (Akoh *et al.*, 2021), medical implants are prosthetics (devices or tissues) intended to replace missing body parts by placing them inside or on the body's surface. Traditional prostheses for load-bearing bone replacement are typically made from metallic materials such as titanium, cobalt chromium alloy, or stainless steel. It poses a significant challenge in orthopaedics, necessitating the development of innovative solutions for bone replacement (Poliakov *et al.*, 2019). They may not always provide optimal outcomes in cases of bone atrophy due to issues like stress shielding and lack of biocompatibility, such as the necessary biological properties to promote bone growth and integration with the surrounding tissue (Cabezas-Villa *et al.*, 2018). Recently, there has been a growing interest in exploring biocomposite prostheses as potential alternatives to tailor the

structural material for their favourable biomechanical properties and potential for promoting bone regeneration (Krishna and Suresh, 2022). Biocomposite prostheses are engineered materials comprising of a combination of materials, typically a metal matrix reinforced with fillers such as ceramics or bioactive agents. These composite structures can provide mechanical support, long-term stability and functionality in a favourable environment for new bone formation by mimicking the natural structure of bone, making them ideal for load-bearing bone replacement and repair (Oshkour *et al.*, 2015). Many researchers have reported the substitution of different composite structures for bone repair and replacements, which include functionally graded composites (Batin *et al.*, 2011; Shahrjerdi *et al.*, 2011; Afzal *et al.*, 2012 and Qian *et al.*, 2015), porous composite structures (Arifin *et al.*, 2017; Zakaria *et al.*, 2018; Zakaria *et al.*, 2021; and Choy *et al.*, 2015) and dense composites (Arif *et al.*, 2017; Sikora-Jasinska *et al.*, 2017; Saba *et al.*, 2018 and Jeong *et al.*, 2020) using biocompatible materials.

However, selecting suitable prostheses with adequate strength, stiffness, and load transfer properties is essential for withstanding the physiological loads experienced by the implant. A radar and spider chart is a graphical method to select materials and process parameters in machining and

*Corresponding author: ibrahim.kh@unilorin.edu.ng

doi: <http://dx.doi.org/10.4314/njtd.v21i1.2174>

manufacturing industries (Holota *et al.*, 2015; Porter and Niksiar, 2018). This chart displays multivariate data as a two-dimensional chart of three or more quantitative variables represented on axes starting from the same point (Wan *et al.*, 2013). The relative position and angle of the axes in the radar chart provide the deviation degree of the actual value and the reference value of each index as required for the selection implant in the load-bearing application. In selecting a load-bearing prosthesis, the prostheses' mechanical strength, stiffness, and fracture toughness must be carefully considered and should have a similar or close modulus to the natural bone to ensure long-term stability (Moghadas *et al.*, 2022), minimise stress-shielding effects and promote proper load transfer to the surrounding tissue (Bahraminasab and Farahmand, 2017). The physical properties of biocomposite implants, including density, porosity, and surface characteristics, have been reported (Oleiwi *et al.*, 2015). Porosity allows for cellular infiltration, nutrient transport, and the formation of new bone within the prosthesis structure (Soro *et al.*, 2018). The optimal porosity range for biocomposite prostheses must be carefully evaluated to ensure successful bone ingrowth without compromising the mechanical integrity of the implant (Wo *et al.*, 2020). Choy *et al.* (2015) revealed Ti/CaP biocomposites with a 1.67 atomic ratio have a porosity of 26%, pore size up to 152 μm , compressive strength of 212 MPa and compressive modulus of 12 GPa. Wo *et al.* (2020) reported the micro-pore structure of porous Ti-6Al-4V scaffolds (pTi) produced by 3D printing. The average pore size and porosity of pTi were obtained in the range of $300 \pm 9 \mu\text{m}$ - $804 \pm 10 \mu\text{m}$ and 42.7 ± 1.1 - $58.9 \pm 1.3\%$, respectively. The pTi facilitated the adhesion and differentiation of osteoblast when pore size decreased or porosity increased. Taniguchi *et al.* (2016) reported that the porous Ti-6Al-4V implants fabricated from additive manufacturing with a porosity of 65% and pore size of 600 μm had better fixation ability and more significant bone ingrowth than those with pore sizes of 300 and 900 μm . Cetinel *et al.* (2019) fabricated Ti foams using the space holder method for bone substitute materials. The result shows that the foam samples with ~60% porosity had compressive strength comparable to that of cortical bone, and the samples with ~80% porosity displayed compressive strength similar to that of cancellous bone. However, the pore size and distribution complexity affected the strength, especially the implants applied for load-bearing bone replacement. The pore distribution analysis is a critical aspect of designing biocomposite implants. It is considered a key measure in many engineering calculations to quantify the complex geometry of the pore space (Oliveira *et al.*, 2020; Safari *et al.*, 2021).

This composite amalgamates titanium's structural durability with hydroxyapatite's bioactivity and osteoconductivity, while calcium carbonate provides potential benefits for controlled biodegradation. It exhibits a versatile range of properties, making it a compelling candidate for developing prosthetic solutions for bone atrophy. Therefore, this study aims to conduct a selection analysis of biocomposite implants by considering the suitable biomechanical and physical properties for load-bearing bone replacement.

II. MATERIAL AND METHODS

A. Preparation of Materials

The commercial pure titanium (P-Ti) powder (99.3% Ti, 0.25% O, 0.1% C, 0.015% H, 0.03% N and 0.3% Fe) was obtained from Eternal Bliss Alloy Casting and Forging, China. The medical grade CaCO₃ (40.75% Ca, 10.98% C, and 48.03% O), binder (Polyvinyl Alcohol) and lubricant (Palm stearin) were obtained in a chemical shop at Tipper Garage, University of Ilorin Road, Tanke, Ilorin, Nigeria. The cow bone-based hydroxyapatite (CB-Ha) biomaterial was prepared from mature cow bone 4 years of age and obtained from the Ipata market, Ilorin, Kwara State. The collected cow bones were washed thoroughly, boiled at 100 °C with distilled water, degreased in acetone, and deproteinised with 1M HCl for 3 hours, as Barua *et al.* (2019) demonstrated. The deproteinised pieces were oven-dried at 70 °C for 48 hours, calcined in a muffle furnace at 1000 °C for 6 hours, and cooled in air. The calcined bones were pulverised into finer particles in a ball mill, obtaining the average particle grain size of ~20 μm using a sieve shaker. The chemical composition was obtained from XRF analysis with 60.01% (PO_4^{3-}) and 39.03% Ca.

B. Fabrication of Biocomposite Implants

The powder metallurgy technique produced the biocomposite specimens in different material structural patterns, including dense, porous and gradient biocomposites. The biocomposite samples were fabricated based on the optimal formulation composition (68.36Ti -18.361Ha - 8.18CaCO₃) obtained from the D-optimal Mixture design of experiment (DM-DOE) for P-Ti (50-100 vol %), CB-Ha (0-45 vol %), CaCO₃ (0-20 vol %) and constant volume fraction PVA (3.9 vol %) as the binder, stabiliser (1 vol %) and lubricant (0.2 vol %) using Design Expert statistical tool. The biomaterial powders were mixed and blended using a Jar mixer for 20 min. Subsequently, the powder blends were transferred into the fabricated cylindrical die with dimensions of 30mm height, 20mm internal diameter and 30 mm outer diameter. The mixtures were uni-axially compacted using a WEIBER P100HE electrically operated hydraulic press under a pressure of 400 MPa for 30 min. The compacted sample was ejected to obtain green biocomposite and preheated at a temperature of 200 °C to remove binder (PVA) and lubricant, as Arifin *et al.* (2014) reported. The wall of the circular die mould and the top punch of the hydraulic press was adequately lubricated to prevent the specimen from sticking to the wall during ejection. The ejected samples were sequentially cleaned in deionised water and dipped in acetone to eliminate contaminants. The preheated green biocomposite samples were further sintered at 800 °C for two hours in a muffle furnace at a heating rate of 10 °C/min. Similar procedures were adopted for the fabrication of porous biocomposite specimens. However, the space holder (SH) method was utilised to fabricate porous biocomposite samples with reported ranges of space holders in the literature for optimal porosity (Cetinel *et al.* 2019). The fabrication involved the mixing of biomaterial compositions of 68.62 Ti- 26.19 (Ha+CaCO₃) with 0.224% of ammonium bicarbonate (100 μm particle size) as space holder (SH) material and decomposed at 110 °C. Then, pour into a cylindrical die mold after adding

stabiliser, lubricant, and binder. The green porous samples were compacted and sintered. The gradient biocomposite (GB) sample was produced from the different compositions (100Ti, 68.36Ti - 18.361Ha - 8.18CaCO₃ and 68.62Ti - 26.19(Ha+CaCO₃) - 0.224SH biomaterial powders and separately poured in the die mould of 20 mm internal diameter and 30mm height dimensions after blending processes using SNE FOURE 28A2092 Jar Mixer, for 20 minutes. 3 separate layers formed were stacked and compacted uni-axially using WEIBER P100HE electrically operated hydraulic press with 400 MPa to obtain green-gradient composite biomaterial samples.. The green-graded biocomposite samples were finally sintered at 800 °C temperatures for two hours in a Muffle electric furnace.

C. Determination of Biomechanical and Physical Properties of Biocomposites

The compression test was conducted following ASTM 3039-79 standards using a 100 KN capacity computerised Testometric universal testing machine (UTM) with specifications: UTM Testometric FS5080, DBBMTCL-5000Kg, Serial No: 38140, Rochdale England). The specimens were cut to a standard dimension of 3.142 x 20² x 10 mm² to conform to the instrument's specification. Three specimens were tested per sample, and the loads at which failure occurred and the deflections shown on the output display unit of the machine were recorded. An average value of the results was calculated for each test sample. The load and deformation readings were automatically recorded until the sample ruptured. The specimen's total surface area, compressive strength and modulus were calculated using a formula adopted by Li and Zhou (2021) and Abutu *et al.* (2018) as follows, respectively.

$$\text{Total Crosssectional Area (CA)} = \pi r^2 h \quad (1)$$

$$\text{Compressive Strenght (CS)} = \frac{\text{Max.Applied Load (AL)}}{\text{Total Crosssectional Area (CA)}} \quad (\text{MPa}) \quad (2)$$

$$\text{Modulus (E)} = \frac{\text{Compressive Stress (CS)}}{\text{Compressive Strain (}\epsilon\text{)}} \quad (\text{GPa}) \quad (3)$$

The Hardness test was carried out to determine resistance to the indentation following ASTM E-92 with Digita Micro Vickers Hardness Tester, HVC-30E model. The test was carried out at three different points for each specimen, and the average value was recorded. The tester is equipped with a monitor to display the microscopic view of the sample surface to accurately determine the indentation surface area that is impressed on the sample. The load of 2 kg was gradually applied and sustained for 15 s, after which the load was removed, and the stage clamp holding the sample was returned to the microscope measuring objective. The impact test was carried out using a Charpy impact testing machine with a capacity of 150J/300J and 2 Joules of minimum value of scale graduation (Avery-Denison, model No: 6705U/33122, Leeds, LS102DE England). The specimens were then subjected to a machining process according to the ASTM E23 testing procedure, with a specimen size of 55 X 10 X 10 mm with a notch angle of 45, 2 mm depth and 0.25 mm radius along the base, as shown in Figure 1 (Li and Zhou 2021). The impact strength values were considered the initiation fracture

toughness (IS), and the plane strain fracture toughness (FT) was calculated from the expression in Eqn. 4 using the single specimen method described in ASTM E1820-08 (Jelitto and Schneider, 2019; Čamagić *et al.*, 2019):

$$FT = \sqrt{\frac{IS \cdot E}{1 - \nu^2}} \quad (4)$$

where FT = fracture toughness (MPam^{0.5}), IS = impact strength (KJ/m²) E = modulus (GPa) and ν = poison ratio.

The density of the sintered samples was investigated using Archimedes' principle following the ASTM B962 standard, and the porosity was calculated mathematically (Zakaria *et al.*, 2021). Suitable biocomposites were selected for application in load-bearing bone replacement using a radar chart component.

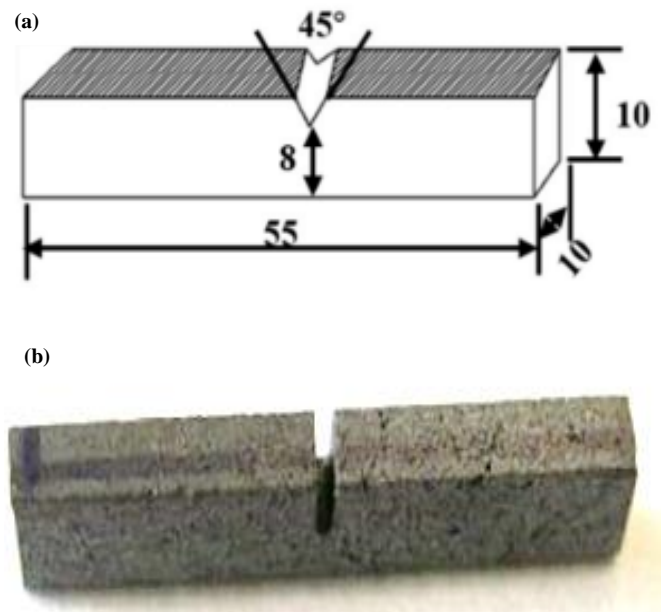


Figure 1: (a) Schematic Standard with dimension. (b) Sample for experimental investigation of impact strength.

D. Characterisation and Pore Distribution Investigation

The samples were characterised on Zeiss Ultra PLUS FEG scanning electron microscope (SEM) using the Oxford instruments detector and Aztec 3.0 software SP1. The SEM micrographs were imported for the analysis and examined for porosity and pore size distribution analysis using an open-source image processing software (ImageJ 1.42). The porosity was determined using the image volume method, to sum up the porosity pixels of all analysed images and divide that value by the sum of the areas observed in these images. Then, this obtained value was multiplied by 100%. These calculations have been conducted without taking into account those areas which are revealed in the segmented images. Image processing has been utilised to evaluate the biophysical parameters such as porosity and pore size distribution (Safari *et al.* 2021). By establishing porosity from routine core analysis as expected results, the porosity volume obtained from image processing is compared with the pore volume of bone established in the literature (Morgan *et al.* 2018).

III. RESULTS

A. Biomechanical and Physical Properties of Biocomposites

The biomechanical properties of dense, porous, and gradient biocomposites are crucial in determining their suitability as implants to replace bone. The results of various biomechanical properties, including compressive strength, modulus, hardness, impact strength, and fracture toughness, are shown in Figure 2. The dense biocomposites exhibited higher mechanical properties at 164.23 MPa than porous biocomposites at 149.29 MPa. In contrast, porous biocomposites tend to have low compressive strength due to the presence of voids. The findings were consistent with the finding of Mara (2015) for biocomposite compressive strength obtained as 167 MPa. The compressive strength of porous biocomposites varied depending on the porosity and pore size distribution (Arifin *et al.*, 2017).

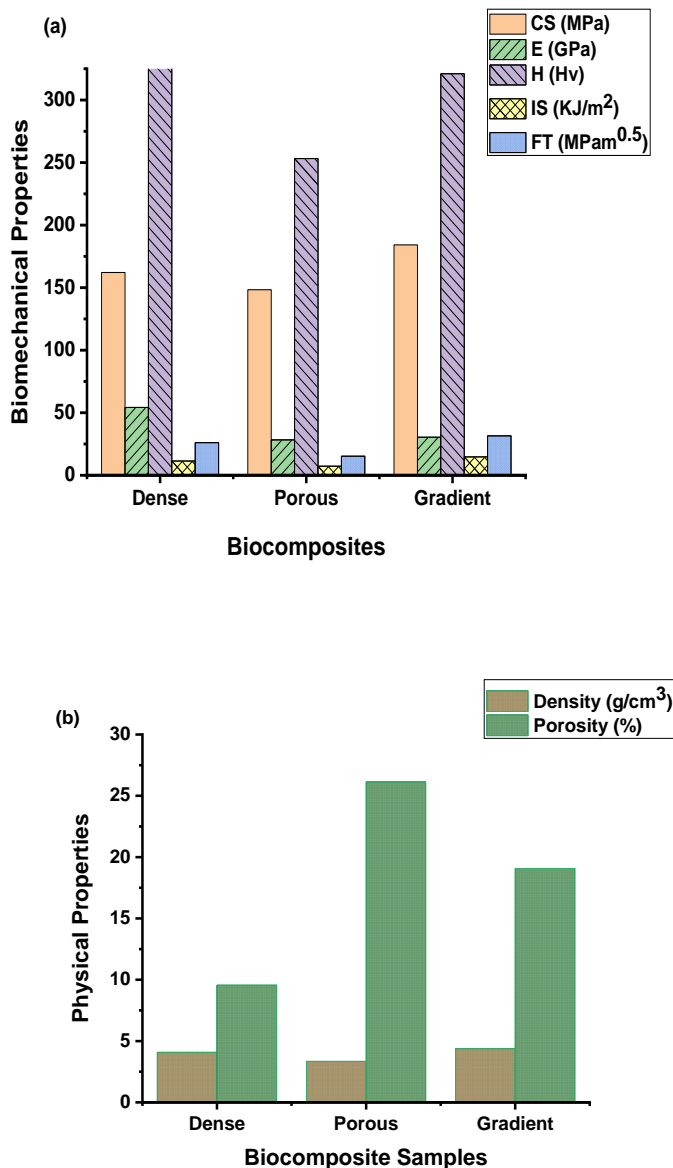


Figure 2: (a) Biomechanical and (b) Physical Properties of Different Structure Ti-Ha-CaCO₃ Biocomposites

The presence of pores in porous biocomposites acted as stress concentrators, making it more susceptible to crack propagation. The fracture toughness of biocomposites influenced by factors such as pore size, porosity, and the presence of toughening agents or reinforcement phases. However, it has been established that biomechanical properties depend on varying factors such as material composition, fabrication techniques, and processing parameters. And customisation of these properties is often necessary to match the requirements of specific bone replacement applications.

A high level of material density and minimal porosity typically characterises dense biocomposites. These characteristics contribute to their superior compressive strength, making them suitable for load-bearing applications. Due to their high compressive strength, dense biocomposites provide stability and support for bone replacement. The transition from dense to porous regions in functionally graded biocomposites allows for a controlled distribution of mechanical properties, enabling optimised load transfer and stress distribution (Bahraminasab and Farahmand, 2017). The compressive stress–strain plot of the dense, porosity and gradient biocomposites samples are presented in Figure 3. The graph shows an initial elastic deformation phase followed by a peak with almost constant flow stress up to significant strains. Conversely, high compressive strength is directly proportional to the highest elastic region in the stress–strain plots (Figure 3). The compressive strength was considered to be the stress value at which the elastic region passes to the plastic deformation (Seramak *et al.*, 2019).

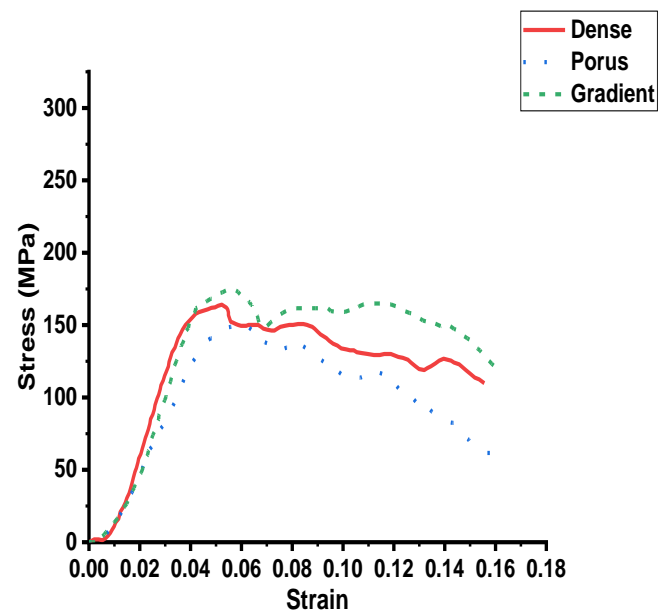


Figure 3: Stress-Strain Plot for the Biocomposite Prostheses

All the peak regions were observed following maximum peak stresses, which suddenly dropped before the start of the peak stage. The maximum peak compressive strengths were around 283.0 MPa for dense pure titanium, while 164.23 MPa,

149.29 and 174 MPa were obtained for dense, porous, and gradient biocomposites. This indicates all the biocomposite samples have better bone compressive strength because the values fall within 2 to 200 MPa, which is consistent with the ranges of the compressive strength of composites reported by Niespodziana (2019); Batin *et al.* (2011). However, the elastic modulus generally decreased for porous biocomposites with 28.3 GPa as the minimum modulus, and it is within the range of cortical bone modulus (7-30 GPa) as reported by Nawawi *et al.* (2011); Prasad *et al.* (2017); Cummings, (2017).

In any case, it can be observed that an increase in reinforcement like the hydroxyapatite and CaCO₃ contents utilised in this study, decreases the material's strength titanium composites, and this agrees with the Arifin *et al.* (2014); Qian *et al.* (2015); Balbinotti *et al.* (2011); Choy *et al.* (2015); Niespodziana, (2019); Saxena *et al.* (2019); Zakaria *et al.* (2021) findings. However, the dense and porous composite structure also contributed to the decrease in strength (Niespodziana, 2019; Prakash *et al.*, 2020; Zakaria *et al.*, 2021), while gradient structure led to strength improvement (Batin *et al.*, 2011). The Young's moduli of metallic materials used for bone replacement range from ~110 GPa for titanium and its alloys to ~190 GPa for stainless steel and ~210 GPa for Co-based alloys, and thus is much higher than the modulus of human cancellous bone (<3 GPa) or compact bone (12-17 GPa) (Batin *et al.*, 2011). However, the results revealed that the gradient specimen has higher compression strength due to the sample's layers arrangement. The sintered porous composite shows early failure in compressive loading due to structural porosity and large pore size. The large pore size acted as a notch, and the crack propagates easily. The compressive strength of the porous Ti-Ha-CaCO₃ composite decreased with the increase in pore size (Prakash *et al.*, 2020). Apart from porous structure and proper interconnection between pores, it possesses moderate strength and appropriate stiffness to achieve satisfactory implants like cortical bone stiffness to avoid the stress shielding effect. A further rise in porosity will probably cause a decrease in compressive strength to match properties like the properties of bones. Therefore, controlling the share of porous agent and compaction pressure can impact porosity and, hence mechanical properties of composites (Niespodziana, 2019).

B. Selection Analysis of Biocomposite Implants

A radar chart component was applied to manufactured biocomposite implants with biomechanical and physical properties obtained for the specimens (Dense, Porous and Gradient Biocomposites). In selecting biocomposites, the data obtained for the mechanical and physical properties of the biocomposites were compared with the cortical bone and titanium data obtained from the literature, as shown in Table 1.

However, the radar charts are effective only if they check limited samples' properties, not more than eight (Holota *et al.*, 2015). After obtaining the properties of both the biocomposites, cortical bone and titanium, the intervals of physical variables for used materials were set for compressive strength (CS), modulus (E), hardness (H), impact strength (IS), fracture toughness (FT), density (D) and porosity (P).

The prepared table of intervals for the individual parameters of the materials with the respective markings (1 to 5) is shown in Table 2. The first column indicates the marking of a variable with a range of variables determined from 1 to 5 (dimensionless number), where 1 represents the lowest value of individual variables, and 5 represents the highest value of variables. According to Table 2, the individual parameter values of the studied mechanical and physical properties were represented with appropriate nodes from 1 to 5. The same nodes are applied based on the biocomposites, titanium and cortical bone properties from Table 1. The nodes for each interval in Table 2 were identified for the properties of the studied biomaterials shown in Table 3, which were used to construct radar charts in Figures 5 to 7.

In the evaluation of the radar chart, it can be observed that the biocomposites have different biomechanical and physical parameters. Dense, porous and gradient materials are similar only in one or two of the required parameters with cortical bone (required) characteristics defined in Table 1. In the selection of biocomposite for replacement of bone or titanium implant, the mechanical and physical properties of dense Ti-Ha-CaCO₃ biocomposite were compared with cortical bone and titanium implant shown in Figure 4. The result revealed that the dense biocomposite compressive strength (164.23 MPa) and porosity of 9.56 percentage values were within the range of cortical bone compressive strength and porosity properties, as reported in Table 1.

Table 1: Biomechanical Properties of Cortical Bone and Titanium Implants

Properties	Titanium	Cortical bone
CS (MPa)	250-600 (Tharaknath <i>et al.</i> , 2016)	100-230 (Nawawi <i>et al.</i> , 2011; Prasad <i>et al.</i> , 2017)
E (GPa)	100-110 (Petersen 2014)	7-30 (Nawawi <i>et al.</i> , 2011; Prasad <i>et al.</i> , 2017)
H (Hv)	244.7-275.3 (2400-2700 MPa) (Kaivosoja <i>et al.</i> , 2013)	50-100 (Hamandi <i>et al.</i> , 2022)
IS (KJ/m ²)	25 (Jelitto and Schneider 2019)	6 (Abdel-Wahab and Silberschmidt, 2011)]
FT (MPam ^{1/2})	60 (Nawawi <i>et al.</i> , 2011)	2-12 (El-Hajje <i>et al.</i> , 2014; Nawawi <i>et al.</i> , 2011; Nurul Amin <i>et al.</i> , 2022)
D (g/cm ³)	4.4-4.51 (Petersen, 2014)	1.8-2.1 (Zakaria <i>et al.</i> , 2018; Nurul Amin <i>et al.</i> , 2022)
P (%)	0-1.46 (Prakash <i>et al.</i> , 2016; Mara, 2015)	5-15 (Morgan <i>et al.</i> , 2018)

Although the biocomposite hardness is within the range of the hardness value of titanium implants, its properties are less than the value of titanium. These characteristics contribute to their superior compressive strength, making them suitable for load-bearing applications. The high impact strength of dense biocomposites can withstand sudden loads and impacts encountered in load-bearing bone replacement applications. Choy *et al.* (2015) reported a similar result however, the modulus of the dense biocomposite is 55.72 GPa which was found to be higher than the modulus of the cortical

bone and it is liable to stress shielding effect due to the mismatch of the biocomposite modulus with bone modulus.

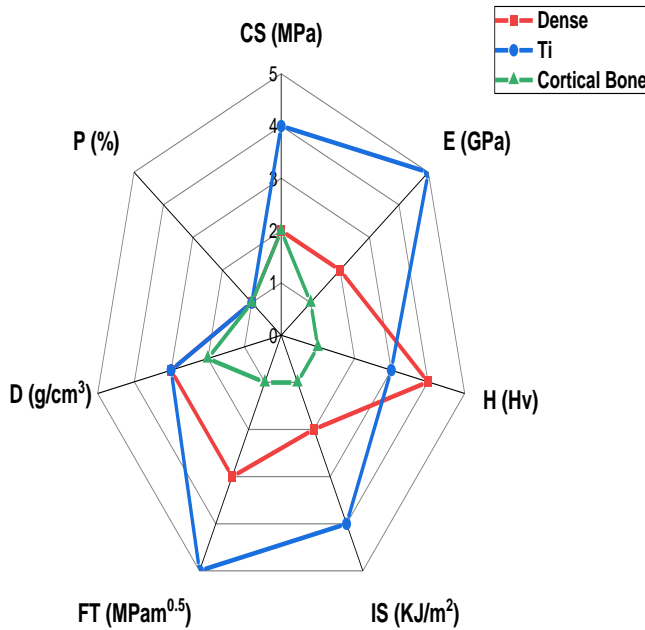


Figure 4: Radar Component Chart for Selection Analysis of Dense Ti-Ha-CaCO₃ Biocomposites

biocomposites are affected by the values which could result from increasing porosity and pore size. The mechanical strength of porous biocomposites may be adjusted by optimising the porosity and pore size using a space holder to balance mechanical properties and biological performance. Cetinel *et al.* (2019) reported porous titanium possesses a porous structure with interconnected voids, which can facilitate tissue ingrowth and promote osseointegration. However, high porosity in the structure of prostheses affects the strength and can lead to premature failure after clinical implantation (Arifin *et al.*, 2017). According to the results from the selection analysis in Figure 6, gradient biocomposite has proved to be the most suitable for replacing titanium implants as an alternative biocompatible prosthesis with strength, stiffness and fracture toughness values, which most closely approximate cortical bone set parameters.

Adoba *et al.* (1997) established that the strength, stiffness, fracture toughness, density and porosity as crucial properties in load-bearing bone replacement, selection of gradient biocomposite in the radar plot has excellent strength, hardness, fracture toughness and optimal porosity. This result suggests the closeness of the modulus prevents bone resorption resulting from stress shielding (Cabezas-Villa *et al.*, 2018). The results indicated that a gradient in pore size reduced stress concentrations at the implant-bone interface, leading to improved load transfer and reduced risk of implant failure. The study emphasised optimising the pore size distribution in gradient structure prostheses to enhance their mechanical performance.

Table 2: The Biomechanical and Physical parameters Interval for studied implants

Node	CS (MPa)	E (GPa)	H (Hv)	Jc (KJ/m ²)	K _{IC} (MPam ^{0.5})	ρ (g/cm ³)	P (%)
1	0-99	1-30	1-100	1.0-7.5	1-12	0-1.5	0-15
2	100-230	31-60	101-200	7.6-14.0	13-25	1.6-3.0	16-30
3	231-360	61-90	201-300	14.1-20.5	26-38	3.1-4.5	31-45
4	361-490	91-120	301-400	20.6-26.0	39-52	4.6-6.0	46-60
5	491-620	121-150	301-500	26.1-32.5	53-65	6.1-7.5	61-75

Table 3: Interval Node for the Selection of Individual Implant Properties.

Parameters	Dense	Porous	Gradient	Titanium	Cortical Bone
CS (MPa)	2	2	2	3-5	2
E (GPa)	2	1	1	5	1
H (Hv)	4	3	4	3	1
Jc (KJ/m ²)	2	2	3	4	1
K _{IC} (MPam ^{1/2})	3	2	3	5	1
ρ (g/cm ³)	3	3	3	3	2
P (%)	1	2	2	1	1

Figure 5 displayed the radar component plot to compare porous Ti-Ha-CaCO₃ biocomposite properties with cortical bone and Titanium implant properties. The plot revealed that the compressive strength (149.29 MPa) of porous biocomposite is within the range of cortical bone porosity percentages, making it suitable for replacing load-bearing bone such as femoral, knee and ankle bone.

However, the presence of pores often leads to a reduction in compressive strength, modulus and density compared to dense biocomposites cortical bone. The compressive strength, impact strength and fracture toughness of porous

These findings contribute to developing biocomposite implants that can effectively replace load-bearing bones while promoting osseointegration and long-term functionality. Gradient biocomposites exhibit a gradual transition in material properties, including porosity and pore size, along their structural gradient. The compressive strength of gradient biocomposites can vary based on the specific design and material composition (Sedighi *et al.* 2017).

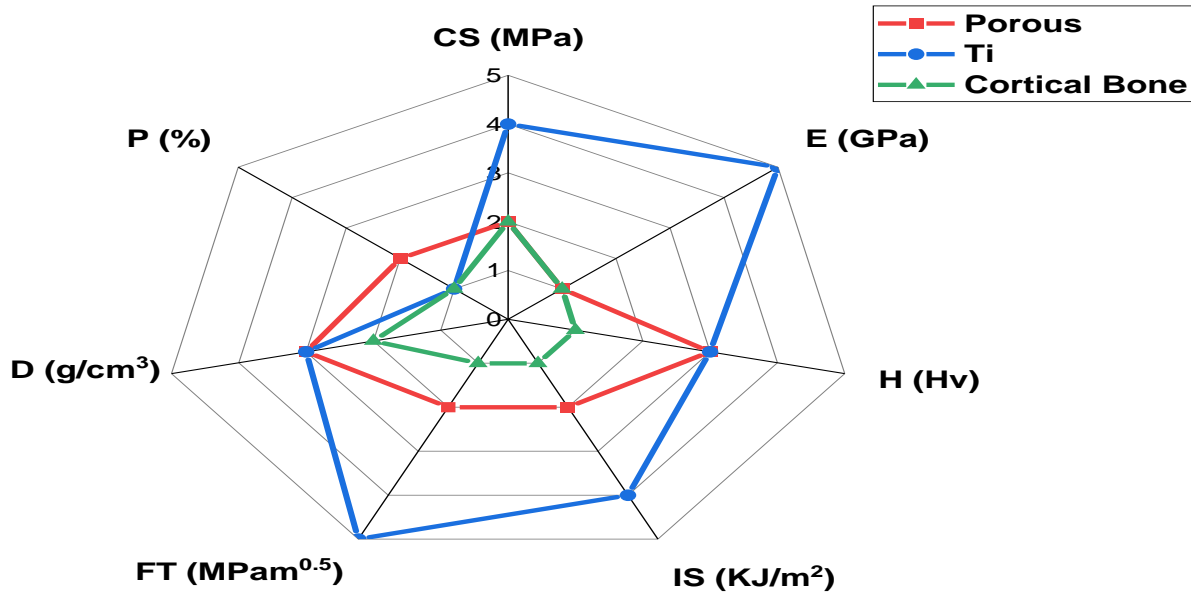


Figure 5: Radar Component Chart for Selection Analysis of Porous Ti-Ha-CaCO₃ Biocomposite

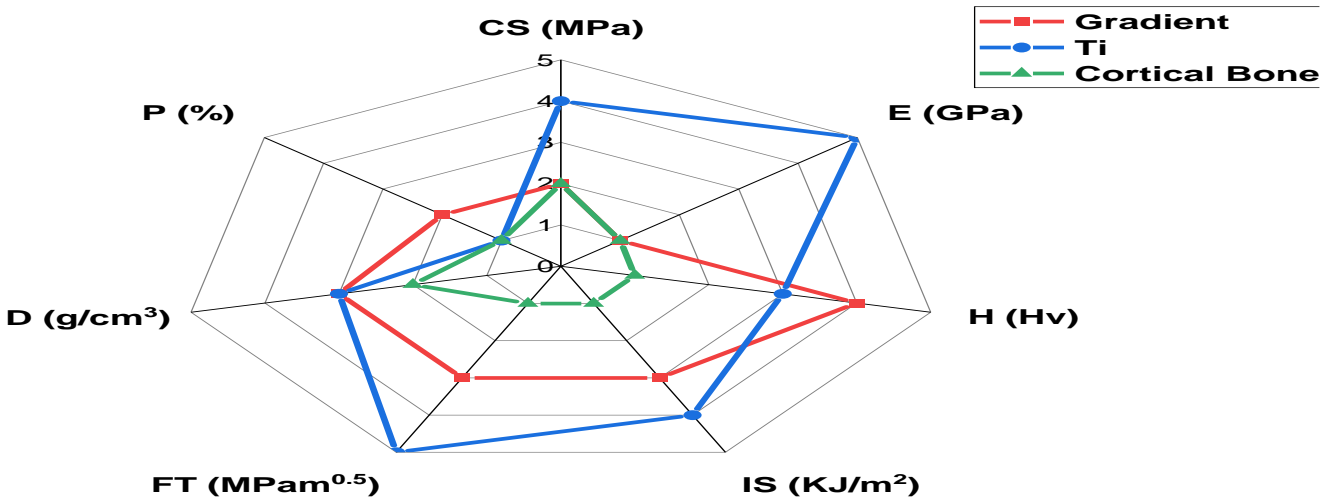


Figure 6: Radar Component Chart for Selection Analysis of Gradient Ti-Ha-CaCO₃ Biocomposite

C. Characterisation of the Biocomposites

The microstructures of the dense, porous and gradient biocomposites examined by SEM analysis are shown in Figure 7. The dense biocomposite microstructure revealed some scratches with little pores due to the reaction of CaCO₃ at very sintering temperatures that usually give up CO₂ and then form pores on the surface of the biocomposite (Choy *et al.*, 2015). The porous and gradient samples showed relatively large irregular pores, with some fine spherical pores uniformly distributed along the surface of the first and second layers of the gradient sample, as shown in Figure 7C. The findings were also confirmed on Image J software by applying a threshold to reveal the porosity and pore distribution pattern shown in Figure 8. Figures 9A, 9B and 9C summarise the measured porosity and average pore size obtained from image J software for the three biocomposites.

The porosity increased with the addition of SH and the measured porosities of the biocomposites were 9.2, 25.72 and 20.62%, respectively, and were significantly higher than the

pure titanium implant with a porosity of 1.46 as obtained by Mara (2015). Regarding dense Ti-Ha-CaCO₃ biocomposites, the emphasis is on achieving a minimum pore size and high density for load-bearing applications. The implant exhibited less than 5% porosity and had a pore size distribution within the submicron to micron range. The average pore sizes of the fabricated porous biocomposites were reported to range from 100 μm to 300 μm. The specific pore size was adjusted by varying the particle size of CaCO₃ and the processing parameters (Choy *et al.*, 2015).

It can be observed from Figure 8 (A, B, C) that there are some large irregular pores in the porous and gradient biocomposite with pore sizes of 252 and 135 μm. The formation of the large pores may be due to the space holder and emission of CO₂ gases produced by the reactions between CaCO₃ and Ti-Ha powders during the sintering process (Choy *et al.*, 2015). Moreover, the pore structure of the implant, including porosity and pore size, is an important characteristic that influences the physical performance of a biomaterial since

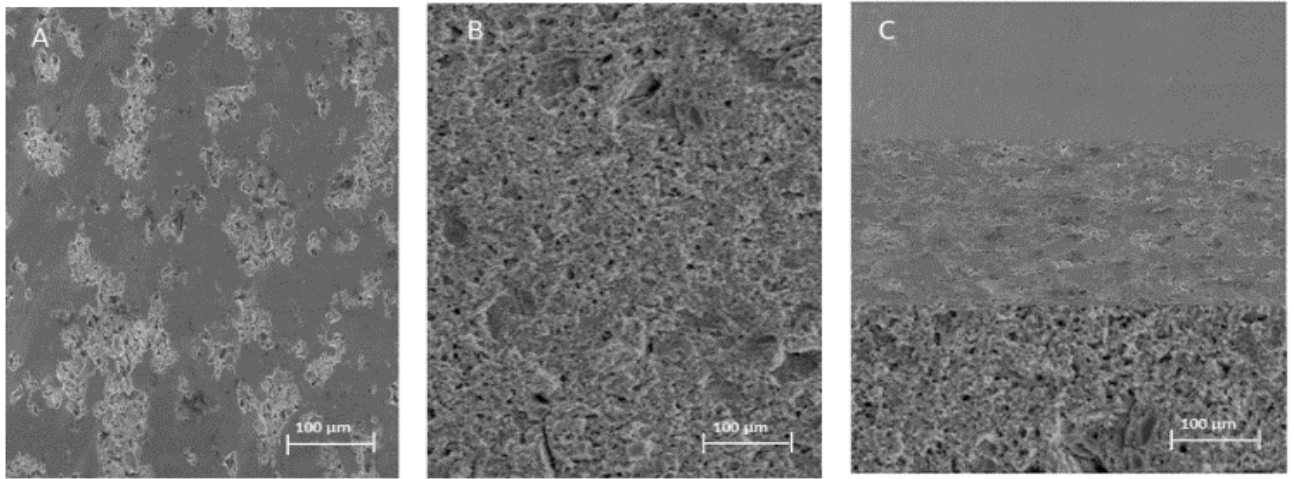


Figure 7: SEM for the Biocomposite Samples: Dense (A), Porous (B) and Gradient (C)

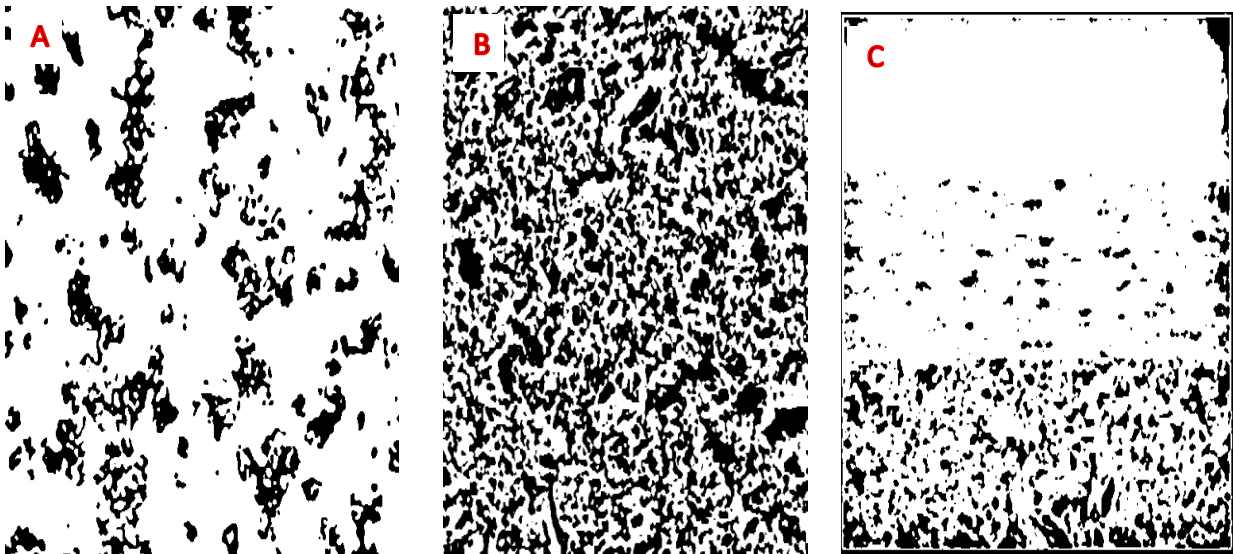


Figure 8: Threshold image of Biocomposites SEM obtained from Image J Software

it allows the migration and proliferation of osteoblasts, mesenchymal cells and vascularisation (Cetinel *et al.*, 2019; Wo *et al.* 2020). The results showed that increasing the porosity of the scaffolds led to decreased mechanical strength but improved the implant's ability to support cell ingrowth and vascularisation. Figure 9 shows the pore size distribution of the studied biocomposite, and it can be observed that the porosities were found to be 9.2%, 27.725 and 20.67% for dense, porous, gradient biocomposites. The porosity obtained agrees with the experimental percentage porosity.

Several studies have investigated the effect of porosity and pore size on the biological behaviour of calcium-phosphate bone grafts, suggesting that the optimal porosity for the bone implant is about 30%. In contrast, a pore size larger than 100 µm is considered most satisfactory for bone graft substitutes to promote implant stabilisation (Choy *et al.*, 2015). This result suggests the closeness of the modulus prevents bone resorption resulting from stress shielding (Cabezas-Villa *et al.*, 2018). The results indicated that a

gradient in pore size reduced stress concentrations at the implant-bone interface, leading to improved load transfer and reduced risk of implant failure. The study emphasized optimising the pore size distribution in functionally graded implants to enhance their mechanical performance. These findings contribute to developing biocomposite implants that can effectively replace load-bearing bones while promoting osseointegration and long-term functionality. Gradient biocomposites exhibit a gradual transition in material properties, including porosity and pore size, along their structural gradient. The compressive strength of functionally graded biocomposites can vary based on the specific design and material composition (Matula *et al.*, 2021).

IV. CONCLUSION

The SEM analysis revealed that the Ti-Ha-CaCO₃ biocomposite implants exhibited a well-defined interconnected porous structure, especially for porous and gradient biocomposites, essential for promoting cell adhesion,

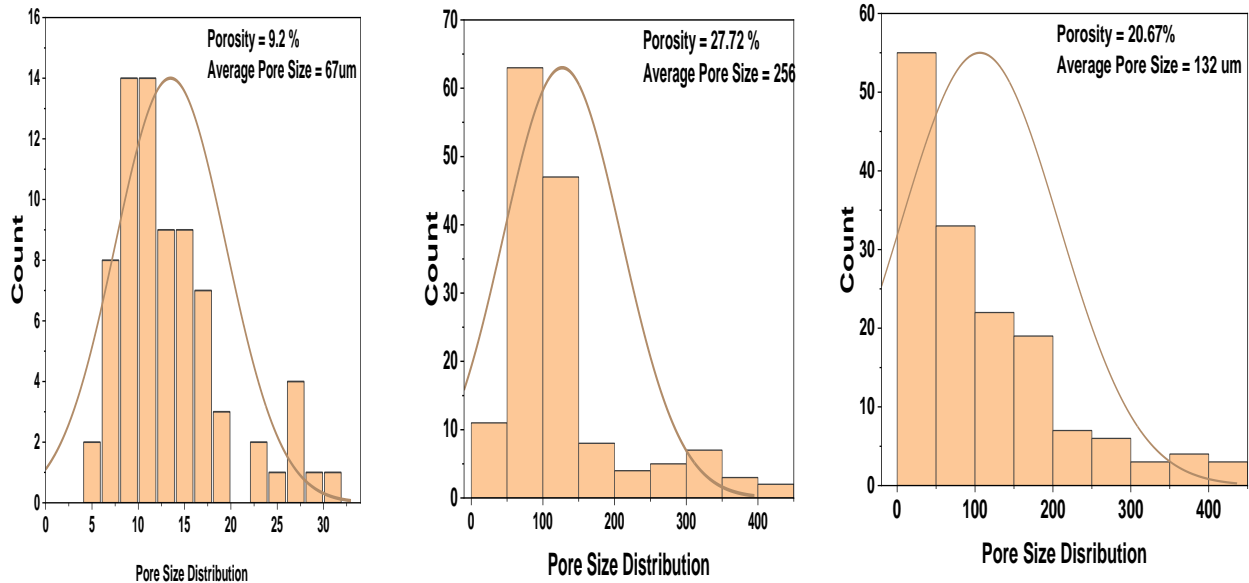


Figure 9: Pore Size Distribution of Ti-Ha-CaCO₃ Biocomposite obtained from Image J Software; Dense (A), Porous (B) and Gradient (C)

proliferation, and nutrient transport within the implant. Moreover, the study measured the porosity percentages of the implants, which demonstrated an optimal porosity range suitable to the gradient and porous biocomposites exhibited desired mechanical properties with porosity of 20.67 and 27.72 % pore size up to 134 and 256 μm, compressive strength of 174 and 149.29 MPa and compressive modulus of 30.42 and 28.3 GPa respectively for load-bearing bone replacement. The controlled porosity contributes to improved mechanical properties, such as load-bearing capacity and elasticity, necessary for withstanding physiological forces and ensuring long-term implant stability. Additionally, the investigation of the mechanical and physical properties of the Ti-Ha-CaCO₃ biocomposite implants through radar chart analysis provided a comprehensive understanding of the material's performance. It favourably showcased a combination of properties in selecting and analysing the biocomposite implants for load-bearing bone replacement. The gradient biocomposite exhibited higher mechanical properties with compressive modulus closer to the cortical bone modulus. And therefore selected as the most suitable biocomposite for replacing bone atrophy.

AUTHOR CONTRIBUTIONS

H. K. Ibrahim: Conceptualization, Methodology, Data curation; Validation, Writing –original draft. **M. S. Abolarin:** Supervision, Resources, Writing – review & editing. **A. S. Abdulrahman:** Supervision, Investigation, Funding acquisition, & editing. **O. Adedipe and U. G. Okoro:** Formal analysis; Writing – review & editing.

REFERENCES

Abdel Wahab, A. A. and Silberschmidt, V. V. (2011). Numerical Modelling Of Impact Fracture Of Cortical Bone

Tissue Using X-Fem. *Journal Of Theoretical And Applied Mechanics*, 49, 3, pp. 599-619, Warsaw 2011.

Abutu, J.; S. A. Lawal; M. B. Ndaliman; R. A. Lafia-Arago; O. Adedipe and I. A. Choudhury. (2018). Effects of process parameters on the properties of brake pad developed from seashell as reinforcement material using grey relational analysis. *Engineering Science and Technology, an International Journal*, 21(4), 787–797. doi:10.1016/j.jestch.2018.05.014

Adoba, A. E.; H. B. McShane; R. D. Rawlings and I. U. Rehman. (1997). Study of the Mechanical Properties and Bioactivity of Functionally Graded Titanium Matrix Composites Reinforced with Bioactive Particles. In *Proceeding: Eleventh International Conference on Composite Materials*, Australian Composite Structures Society Woodhead Publishing Limited, Queensland, Australia.

Afzal M. A. F.; P. Kesarwani and K. M. Reddy. (2012). Functionally graded hydroxyapatite-alumina-zirconia biocomposite: synergy of toughness and biocompatibility. *Mat Sci Eng C* 2012; 32(5): 1164–1173

Akoh, C.C.; J. Chen; R. Kadakia; Y.U. Park; H. Kim and S.B. Adams. (2021). Adverse events involving hallux metatarsophalangeal joint implants: analysis of the United States Food and Drug Administration data from 2010 to 2018. *Foot and Ankle Surgery*, 27(4), pp.381-388.

Arif, S.; M. Alam; A.H. Ansari; M.A. Siddiqui and M. Mohsin. (2017). Study of mechanical and tribological behaviour of Al/SiC/ZrO₂ hybrid composites fabricated through powder metallurgy technique, *Mater. Res. Express* 4, 07651, [https://doi.org/10.1088/Mater. Res. Express 4 \(2017\) 076511](https://doi.org/10.1088/Mater. Res. Express 4 (2017) 076511) 2053-1591/aa7b5f.

- Arifin, A.; A. B. Sulong; A. S. Mohruni and I. Yani. (2014).** Palm stearin as alternative binder for MIM: a review. *J Ocean, Mech Aerosp Sci Eng*, 7, 18-23.
- Arifin, A.; A. B. Sulong; L. C. Fun; Gunawan and Yani, I. (2017).** Porous titanium alloy/hydroxyapatite composite using powder compaction route. *Journal of Mechanical Engineering and Sciences*, Volume 11, Issue 2, pp. 2679-2692, DOI: <https://doi.org/10.15282/jmes.11.2.2017.10.0244>
- Bahraminasab, M. and Farahmand, F. (2017).** State of the art review on design and manufacture of hybrid biomedical materials: Hip and knee prostheses. *ProcIMEchE Part H: J Engineering in Medicine* 1–29. DOI: 10.1177/0954411917705911.
- Balbinotti, P.; E. Gemelli; G. Buerger; S. A. D. Lima; J. D. Jesus; N. H. A. Camargo ... and Soares, G. D. D. A. (2011).** Microstructure development on sintered Ti/HA biocomposites produced by powder metallurgy. *Materials Research*, 14, 384-393.
- Barua, E.; P. Deb; S. Das Lala and A. B. Deoghare. (2019).** Extraction of hydroxyapatite from bovine bone for sustainable development. *Biomaterials in Orthopaedics and Bone Regeneration: Design and Synthesis*, 147-158.
- Batin, G.; C. Popa; L. Brândușan and I. Vida-Simiti. (2011).** Mechanical Properties Of Ti/Ha Functionally Graded Materials For Hard Tissue Replacement. *Powder Metallurgy Progress*, Vol.11 (2011), No 3-4, pp. 206-209
- Cabezas-Villa, J. L.; L. Olmos; D. Bouvard; J. Lemus-Ruiz and O. Jiménez. (2018).** Processing and properties of highly porous Ti6Al4V mimicking human bones. *Journal of Materials Research*, 33(06), 650–661. doi:10.1557/jmr.2018.35
- Cetinel, O.; Z. Esen and B. Yildirim. (2019).** Fabrication, Morphology Analysis, and Mechanical Properties of Ti Foams Manufactured Using the Space Holder Method for Bone Substitute Materials. *Metals*, 9(3), 340. doi:10.3390/met9030340
- Choy, M. T.; C.-Y. Tang; L. Chen; W.-C. Law; C.-P. Tsui and W. W. Lu. (2015).** Microwave assisted-in situ synthesis of porous titanium/calcium phosphate composites and their in vitro apatite-forming capability. *Composites Part B: Engineering*, 83, 50–57. doi:10.1016/j.compositesb.2015.08.04
- El-Hajje, A.; E. C. Kolos; J. K. Wang; S. Maleksaedi; Z. He; F. E. Wiria; C. Choong and A. J. Ruys. (2014).** Physical and mechanical characterisation of 3D-printed porous titanium for biomedical applications. *Journal of Materials Science: Materials in Medicine*, 25(11), 2471–2480. doi:10.1007/s10856-014-5277-2.
- Hamandi, F.; J.T. Tsatalis and T. Goswami. (2022).** Retrospective Evaluation and Framework Development of Bone Anisotropic Material Behavior Compared with Elastic, Elastic-Plastic, and Hyper-Elastic Properties. *Bioengineering* 2022, 9, 9. <https://doi.org/10.3390/bioengineering9010009>
- Holota, T.; M. Kotus; M. Holienčinová; J. Mareček and M. Zach. (2015).** Application of radar chart in the selection of material for clutch plates. *Acta Universitatis Agriculturae et Silviculturae Mendelianae Brunensis*, 63(1), 39-43.
- Jawad K. O.; A. A. Rana and A. M. Sura. (2015).** Fabrication, characterisation and Physical Properties of Functionally Graded Ti/HAP bioimplants, *Wulfenia Journal* Vol 22, No. 7 pp. 336-348.
- Jelitto, H. and Schneider, G. A. (2019).** Fracture toughness of porous materials – Experimental methods and data. *Data in Brief*, 103709. doi:10.1016/j.dib.2019.103709
- Jeong, W.; S.-E. Shin; and H. Choi. (2020).** Microstructure and Mechanical Properties of Titanium–Equine Bone Biocomposites. *Metals*, 10(5), 581. doi:10.3390/met10050581
- Kaivosoja, E.; V.-M. Tiainen; Y. Takakubo; B. Rajchel; J. Sobiecki; Y. T. Konttinen and V. Takagi. (2013).** Materials used for hip and knee implants. *Wear of Orthopaedic Implants and Artificial Joints*, 178–218. doi:10.1533/9780857096128.1.178
- Krishna, E. S. and Suresh, G. (2022).** Bioactive Titanium-Hydroxyapatite Composites by Powder Metallurgy Route, Volume 12, Issue 4, 2022, 5375 – 5383 <https://doi.org/10.33263/BRIAC124.53755383>
- Li, C. and Zhou, Z. (2021).** Charpy Impact Behavior of a Novel Stainless Steel Powder Wire Mesh Composite Porous Plate. *Materials*, 14, 2924. <https://doi.org/10.3390/ma14112924>
- Mara, F. C. V. T. (2015).** Mechanical Characterisation of Porous Titanium Implant Materials, PhD thesis, Universidade do Minho, Escola de Engenharia.
- Matula, I.; G. Dercz; M. Sowa; A. Barylski and P. Duda. (2021).** Fabrication and Characterisation of New Functional Graded Material Based on Ti, Ta, and Zr by Powder Metallurgy Method. *Materials*, 14, 6609. <https://doi.org/10.3390/ma14216609>.
- Moghadas, K.; M. S. M. Isa; M. A. Ariffin; M. Z. Mohd jamil; S. Raja; B. Wu; M. Yamani; M. R. Muhamad; F. Yusof; M. F. Jamaludin; M. S. Ab Karim; B. Abdul Razak and N. Yusoff. (2022).** A review on biomedical implant materials and the effect of friction stir-based techniques on their mechanical and tribological properties, *Journal of Materials Research and Technology*, Volume 17, pp. 1054-1121, <https://doi.org/10.1016/j.jmrt.2022.01.050>.
- Morgan, E. F.; G. U. Unnikrisnan and A. I. Hussein. (2018).** Bone Mechanical Properties in Healthy and Diseased States. *Annual Review of Biomedical Engineering*, 20(1), 119–143. doi:10.1146/annurev-bioeng-062117-121139
- Nawawi, N. A.; A. S. F. Alqap and I. Sopyan. (2011).** Recent Progress on Hydroxyapatite-Based Dense Biomaterials for Load Bearing Bone Substitutes, *Recent Patents on Materials Science*, Volume 4, pp. 63-80.
- Niespodziana, K. (2019).** Synthesis and properties of porous Ti-20 wt.% HA nanocomposites. *Journal of Materials Engineering and Performance*, 28(4), 2245-2255.
- Nurul Amin, A. K. M.; S. N. M. Nasir; N. S. Khalid and M. D. Arif. (2012).** Comparison of Surface Roughness Attainable in High Speed End Milling of Silicon with Air Blowing on Conventional and CNC Milling Machines. *Advanced Materials Research*, 576, 1922. doi:10.4028/www.scientific.net/amr.576.19.

- Oliveira, T. J. A.; F. A. M. Cássaro and L. F. Pires. (2020).** The porous size distribution obtained and analysed by free access software. *Revista Brasileira de Ensino de Física*, vol. 42, e20200192: 1-4, DOI: <https://doi.org/10.1590/1806-9126-RBEF-20200192>.
- Oshkour, A. A.; S. Pramanik; M. Mehrali; Y. H. Yau; F. Tarlochan and N. A. Abu Osman. (2015).** Mechanical and physical behavior of newly developed functionally graded materials and composites of stainless steel 316L with calcium silicate and hydroxyapatite. *Journal of the Mechanical Behavior of Biomedical Materials*, 49, 321–331. doi:10.1016/j.jmbbm.2015.05.020
- Petersen, R. (2014).** Titanium Implant Osseointegration Problems with Alternate Solutions Using Epoxy/Carbon-Fiber-Reinforced Composite. *Metals*, 4(4), 549–569. doi:10.3390/met4040549
- Poliakov A.; V. Pakhaliuk and V. L. Popov. (2019).** Current Trends in Improving of Artificial Joints Design and Technologies for Their Arthroplasty. *Front. Mech. Eng.* 6:4. doi:10.3389/fmech.2020.00004.
- Porter, M. M. and Niksiar, P. (2018).** Multidimensional mechanics: Performance mapping of natural biological systems using permutated radar charts. *PLoS one*, 13(9), e0204309.
- Prakash, K. S.; P. M. Gopal; D. Anburose and V. Kavimani. (2016).** Mechanical, corrosion and wear characteristics of powder metallurgy processed Ti-6Al-4V/B4C metal matrix composites. *Ain Shams Engineering Journal*. doi:10.1016/j.asej.2016.11.003
- Prakash, C.; S. Singh; S. Ramakrishna; G. Królczyk and C. H. Le. (2020).** Microwave sintering of porous Ti-Nb-HA composite with high strength and enhanced bioactivity for implant applications. *Journal of Alloys and Compounds*, 824, 153774.
- Prasad, K.; O. Bazaka; M. Chua; M. Rochford; L. Fedrick; J. Spoor; ... and Bazaka, K. (2017).** Metallic Biomaterials: Current Challenges and Opportunities. *Materials*, 10(8), 884. doi:10.3390/ma10080884.
- Qian, C.; F. Zhang and J. Sun. (2015).** Fabrication of Ti/HA composite and functionally graded implant by three-dimensional printing. *Bio-Medical Materials and Engineering*, 25(2), 127–136. doi:10.3233/bme-151263
- Saba, F.; F. Zhang; S. Liu and T. Liu. (2018).** Reinforcement size dependence of mechanical properties and strengthening mechanisms in diamond reinforced titanium metal matrix composites. *Composites Part B: Engineering*. doi:10.1016/j.compositesb.2018.12.014.
- Safari, H.; B. J. Balcom and A. Afrough. (2021).** Characterisation of pore and grain size distributions in porous geological samples—An image processing workflow. *Computers & Geosciences*, 156, 104895.
- Saraf, S.; A. Singh and B. G. Desai. (2019).** Estimation of Porosity and Pore size distribution from Scanning Electron Microscope image data of Shale Samples: A Case Study on Jhuran Formation of Kachhh Basin, India. *ASEG Extended Abstracts*, 2019(1), 1–3. doi:10.1080/22020586.2019.12073197.
- Sedighi, M.; N. Omid and A. H. Jabbari. (2017).** Experimental Investigation of FGM Dental Implant Properties Made from Ti/HA Composite, *Mechanics of Advanced Composite Structures* 4 (2017) 233-237.
- Saxena, V.; V. Kumar; A. Rai; R. Yadav; U. Gupta; V. K. Singh and P. P. Manna. (2019).** Optimisation of the bio-mechanical properties of Ti-8Si-2Mn alloy by 1393B3 bioactive glass reinforcement. *Materials Research Express*, 6(7), 075401.
- Shahrjerdi, A.; F. Mustapha; M. Bayat; S. M. Sapuan and D. L. A. Majid. (2011).** Fabrication of functionally graded Hydroxyapatite/Titanium by applying optimal sintering procedure and powder metallurgy. *International Journal of the Physical Sciences* Vol. 6(9), pp. 2258-2267, DOI: 10.5897/IJPS11.223.
- Sikora-Jasinska, M.; C. Paternoster; E. Mostaed; R. Tolouei; R. Casati; M. Vedani and D. Mantovani. (2017).** Synthesis, mechanical properties and corrosion behavior of powder metallurgy processed Fe/Mg2Si composites for biodegradable implant applications, *Materials Science and Engineering C*, doi: 10.1016/j.msec.2017.07.049.
- Soro, N.; L. Brassart; Y. Chen; M. Veidt; H. Attar and M. S. Dargusch. (2018).** Finite element analysis of porous commercially pure titanium for biomedical implant application. *Materials Science and Engineering: A*, 725, 43–50. doi:10.1016/j.msea.2018.04.009
- Taniguchi, N.; S. Fujibayashi; M. Takemoto; K. Sasaki; B. Otsuki; T. Nakamura; T. Matsushita; T. Kokubo and S. Matsuda. (2016).** Effect of pore size on bone ingrowth into porous titanium implants fabricated by additive manufacturing: An in vivo experiment. *Materials Science and Engineering: C*, 59, 690–701. doi:10.1016/j.msec.2015.10.069
- Tharaknath, S.; R. Ramkumar and B. Lokesh. (2016).** Middle-East Journal of Scientific Research 24 (Recent Innovations in Engineering, Technology, Management & Applications): 124-132, DOI: 10.5829/idosi.mejsr.2016.24.RIETMA120.
- Wan, Y.; K. Cheng; Z. Liu and H. Ye. (2013).** An investigation on machinability assessment of difficult-to-cut materials based on radar charts. *Proceedings of the Institution of Mechanical Engineers, Part B: Journal of Engineering Manufacture*, 227(12), 1916-1920.
- Wo, J.; S. Huang; D. Wu; J. Zhu; Z. Li and F. Yuan. (2020).** The integration of pore size and porosity distribution on Ti-6Al-4V scaffolds by 3D printing in the modulation of osteo-differentiation, *Journal of Applied Biomaterials & Functional Materials*, Volume 18: 1–10, DOI: 10.1177/2280800020934652
- Zakaria, M.Y.; A.B. Sulong; M.I. Ramli; B. Ukwueze; W.S.W. Harun and R.L. Mahmud. (2018).** Fabrication of Porous Titanium hydroxyapatite Composite Via Powder Metallurgy With Space Holder Method *Journal of Advanced Manufacturing Technology (JAMT)*, Vol. 12 No. 1, pp. 37-48.
- Zakaria, M. Y.; M. I. Ramli; A. B. Sulong; N. Muhamad and M. H. Ismail. (2021).** Application of sodium chloride as space holder for powder injection molding of alloy Titanium-Hydroxyapatite composites. *Journal of Materials Research and Technology*, 12, 478–486. doi:10.1016/j.jmrt.2021.02.087.